Ocean Engineering 136 (2017) 260–271

Contents lists available at ScienceDirect

Ocean Engineering

journal homepage: www.elsevier.com/locate/oceaneng

Dominant parameters for vortex-induced vibration of a steel catenary riser under vessel motion

Jungao Wang[a,b,c], Shixiao Fu[a,b,d,*], Carl Martin Larsen[e], Rolf Baarholm[f], Jie Wu[d], Halvor Lie[d]

[a] State Key Laboratory of Ocean Engineering, Shanghai Jiao Tong University, Shanghai, China
[b] Collaborative Innovation Center for Advanced Ship and Deep-Sea Exploration, Shanghai Jiao Tong University, Shanghai, China
[c] Department of Mechanical and Structural Engineering and Materials Science, University of Stavanger, Stavanger, Norway
[d] SINTEF Ocean, Trondheim, Norway
[e] Department of Marine Technology, Centre for Ships and Ocean Structures, Norwegian University of Science and Technology, Trondheim, Norway
[f] Statoil, Trondheim, Norway

ARTICLE INFO

Keywords:
Vortex-induced vibration
KC number
Maximum equivalent current velocity
Tension variation

ABSTRACT

Recent research has confirmed a new type of vortex-induced vibration (VIV) in steel catenary risers (SCRs), purely caused by vessel motion. Vessel motion-induced VIV occurs because the SCR is exposed to the equivalent oscillating current due to its own motions relative to the still water. Preliminary results indicate that vessel motion-induced VIV is quite different from ocean current-induced VIV and is characterized with distinct time-varying features. In the present study, we aim at further summarizing the dominant parameters that govern the general vessel motion-induced VIV responses. Throughout the comparative studies on the instantaneous and statistical VIV responses including strain, displacement, response frequency, fatigue damage and top tension variation, the maximum Keulegan-Carpenter number KC_{max} and the maximum equivalent current velocity V_{n_max} are found to be the two dominant parameters that govern the vessel motion-induced VIV responses. Generally speaking, when KC_{max} is sufficiently large (larger than 39 according to the present study), the general vessel motion-induced VIV response is dominated by $V_{n.max}$. However, when KC_{max} is small, the VIV response is less time-varying and shows strong correlation with both KC_{max} and the local KC number distribution along the SCR. Vessel motion-induced VIV response frequency models are also reviewed and discussed considering different KC_{max} and $V_{n.max}$ ranges. Hopefully, these results can provide some general guidelines for future vessel motion-induced VIV prediction and for industrial references.

1. Introduction

Compliant risers, such as steel catenary risers (SCRs) and steel lazy wave risers (SLWRs), are recognized as the potential solutions for the deep-water production riser systems because of their ability in tolerating the large wave-induced vessel motions that are encountered in open water (Basim, 2001). However, in the design point of view, these large-amplitude vessel motions would cause considerable fatigue damage to the risers, especially at the touch-down point (TDP) area due to the continuous riser-soil interaction (Quéau, 2015). In addition, vortex-induced vibration (VIV) resulting from the ocean current is the other major contributor to the riser fatigue damage (DNV, 2010a). Marine riser VIV is a fluid-structure interaction problem that has been widely studied numerically and experimentally in recent decades (Baarholm et al., 2006 ; Chaplin et al., 2005; Griffin and Vandiver, 1984; Lie and Kaasen, 2006; Tognarelli et al., 2001; Trim et al., 2005). Nevertheless, most of the studies assume that the current over the riser is time-invariant. Even with such assumption, the VIV response of a long, flexible riser is still quite complex and chaotic (Vandiver et al., 2005).

Recent research has confirmed another type of VIV for the compliant risers under pure vessel motions, known as vessel motion-induced VIV (Grant et al., 1999; Gonzalez, 2001; Liao, 2002; Rateiro et al., 2013). This VIV response is named as heave induced lateral motion (HILM) by Cunff et al. (2005) and is named as vortex self-induced vibration (VSIV) by Fernandes et al. (2008, 2014). Vessel motion-induced VIV occurs because the riser is exposed to the equivalent oscillatory current due to the relative motion between the oscillating riser and the still water particles around (Wang et al., 2014a, 2014b, 2015a, 2015b). We name such oscillatory current as equivalent current because this current is not physically existed in the environmental conditions, but it has an equivalent effect as oscillatory current acting on the risers. It has been experimentally observed that such

* Corresponding author at: State Key Laboratory of Ocean Engineering, Shanghai Jiao Tong University, Shanghai, China; SINTEF Ocean, Trondheim, Norway.
E-mail addresses: shixiao.fu@sjtu.edu.cn, shixiao.fu@sintef.no (S. Fu).

http://dx.doi.org/10.1016/j.oceaneng.2017.03.015
Received 2 May 2016; Received in revised form 21 November 2016; Accepted 12 March 2017

Nomenclature

D	outer diameter [m]
L	test model length [m]
EI	bending stiffness [N m^2]
EA	tensile stiffness [N]
θ	hang-off angle [°]
ε	strain
T_{Axial}	top axial tension [N]
f_n	nth natural frequency [Hz]
A_i	full scale top imposed motion amplitude at real hang-off point [m]
A_{im}	scaled top imposed motion amplitude at real hang-off point [m]
T_i	full scale top imposed motion period at real hang-off point [s]
T_{im}	scaled top imposed motion period at real hang-off point [s]
f_{im}	scaled top imposed motion frequency at real hang-off point [Hz]
KC	KC number
KC_{max}	maximum KC number along the riser
A_n	local oscillatory displacement amplitude [m]
V_{n_max}	maximum in-plane equivalent current velocity [m/s]
A/D	normalized VIV displacement
St	Strouhal number
N	vortex shedding pairs per vessel motion period
f_{resp}	response frequency for vessel motion-induced VIV
f_{domi}	dominant frequency for vessel motion-induced VIV
C_D	drag coefficient
Ca	added mass coefficient

equivalent oscillatory current would generate alternative vortex shedding and lead to considerable riser VIV as well (Sumer and Fredsøe, 1988; Fu et al., 2013a, 2013b). Considering the geometric nonlinearity of the compliant risers, the equivalent flow field under vessel motion is both time- and space-varying, which further results in quite complex vortex shedding processes (Wang et al., 2015b). For example, the time-varying shedding frequency could vary over several of the natural frequencies of the riser within merely one fourth of the vessel motion period. Unresolved issues include determining mode(s) excited in such a short span of time as well as the value of the response amplitude and frequency. An additional complication is that the moving riser would pass through its own wake when it reverses direction. All of these characteristics make vessel motion-induced VIV more complex and difficult to predict.

To further understand vessel motion-induced VIV, Statoil conducted a large-scale model test on a truncated SCR with forced motion at the top of the model (Fu et al., 2013a; Wang 2014a). Previous case study has confirmed that vessel motion-induced VIV was characterized by strongly time-varying features (Wang et al., 2014a, 2015b). Moreover, vessel motion-induced VIV differs considerably for different test cases, as observed in the equivalent flow field, touch down point variation and top axial tension variation. Particularly, for the case where vessel motion is considerably large, VIV during half of the vessel motion period when the vessel is heaving upwards (it is named as 'lift-up' phase according to the vessel motion displacement time history, this will be further illustrated in Fig. 5 in the following context) is found to be quite different from that when the vessel is heaving downwards (it is named as 'push-down' phase). This riser VIV discrepancy inside of one vessel motion period is related to the instantaneous location of the touch down point and axial tension variation (Wang et al., 2015b).

Despite these complicating factors, it is believed that specific analysis can be performed to further reveal certain underlying features or trends for vessel motion-induced VIV. In this paper, we select three group of test cases for comparative study. Based on the comprehensive investigation on the instantaneous and statistical strain, displacement, frequency, fatigue damage and top tension, dominant parameters for vessel motion-induced VIV are identified as maximum KC number $KC_{\max}$ and maximum in-plane equivalent current velocity $V_{n,\max}$. Furthermore, how VIV responses will be affected by these two parameters are suggested. KC number is defined as:

$$KC(s) = \frac{2\pi A_n(s)}{D} \tag{1}$$

where A_n is the local riser motion amplitude normal to its axial axis, and D is the outer diameter of the riser. KC number is a dimensionless number describing the relative importance of the drag forces over inertia forces for bluff objects in the oscillatory flow. In-plane equivalent current velocity V_n is in fact the same as the riser in-plane global motion velocity normal to the riser axial axis.

Hopefully, these results can provide some general guidelines for future vessel motion-induced VIV prediction and for industrial references.

2. Experimental description

The vessel motion-induced VIV model test was carried out in the ocean basin at Shanghai Jiao Tong University. The prototype SCR is a 4100 m long riser operating at the water depth of 1500 m, as configured in Fig. 1. Due to the size limitation of the ocean basin with the dimension of 50 m in length, 40 m in width and 10 m in depth, the riser model has to be scaled accordingly. The scaling strategy is to adopt the correct similarity laws according to the main objective of the presented study, which is to investigate the relationship among the vessel motion, riser global dynamic responses and the associated VIV responses. Therefore, we need to ensure the vessel motion, riser global dynamic responses and the VIV responses in the model scale are similar to what happed in the real scale as much as possible. The model test design is illustrated in Fig. 2 and is explained in detail as follow:

Firstly, due to the difficulties on the small riser model fabrication and fiber strain sensors instrumentation, the outer diameter of the riser model is determined to be around two centimeters. This leads to a scaling factor λ at around 20 based on the geometry similarity, which further scales down the water depth to 75 m in model scale. Therefore, it is decided to truncate the full-length riser into a segment with its vertical length at around 9 m to satisfy the ocean basin test water depth. Finally, a total 23.71 m riser model is truncated, starting from part of the flow line section to the lower part of the riser sag-bend. The comparison between the full-length and truncated riser is also illustrated in Fig. 1. Upper truncation motion time histories are calculated beforehand from the full-length riser, where only harmonic heave

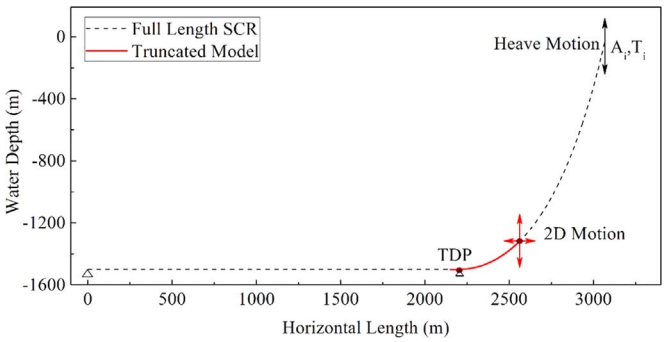

Fig. 1. Geometrical configuration of the full-scale full-length SCR.

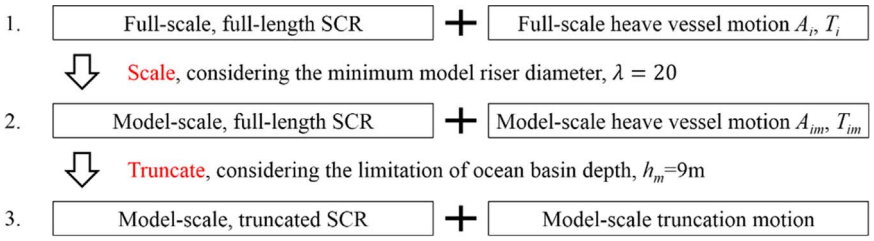

Fig. 2. Mode test design methodology.

motion of a targeted SPAR platform is considered for the purpose of fundamental research. The truncation motion time histories are then scaled according to the Froude similarity to address the vessel motion effect. It should be mentioned that the dynamic similarity is of great significance in the model test design as well (Rateiro et al., 2012). Regarding our vessel motion-induced VIV model test (fundamentally, it is VIV in oscillatory flow), a good replication of the non-dimensional *KC* number distribution along the riser under vessel motion is extremely important, since *KC* number is supposed to be one of the key parameters influencing VIV in oscillatory current (Sumer and Fredsøe, 1988). Our published preliminary research has shown that the truncated riser segment under truncation point excitation responds almost the same dynamically as that in the full-length model under vessel motion (Wang et al., 2015b). This ensures that the *KC* number distribution in the truncated model would be almost the same as that in a full-length riser.

As for the similarities issues considering VIV, there are several gaps, which are hard to overcome. They are summarized and discussed as follow:

1) Ideally, Reynolds number during the model test should be the same as that in the full-scaled scenario. However, due to the adoption of Froude similarity considering the vessel motion, Reynolds number in the full scale (within subcritical to critical region) is $(\sqrt{\lambda})^{3/2}$ times higher than that in the model test (subcritical region). This would not alter the associated hydrodynamic forces dramatically, but we should keep in mind that vortex shedding process might be a bit different.
2) The cross section of the model riser is in fact a composite combination of cooper wire inside and polyethylene (PE) pipe outside to satisfy the mass requirement, and therefore, to ensure the similarity in riser top tension. The philosophy of controlling the stiffness is to maintain the axial stiffness and to reduce the bending stiffness as small as possible, in order to make sure the truncated riser would respond as a tensioned-string as it should be in full-length. We have to admit that these materials and associated physical parameters are not easy to control. However, the riser physical parameters we present in this paper are the best balance we could make at the time. All physical parameters are well-measured and documented though material tests, and they are summarized in Table 1 with comparison to the full-scaled values.
3) The third issue is that due to the length truncation, the model riser would have less damping region compared to the full-length riser. With less damping, a response reflection at both ends of the riser are also expected. Such effects will be further explained in the result and discussion part.

Generally speaking, the truncated test model might not respond to VIV in the same manner as a full-length mode and the associated VIV responses could likely be a bit larger due to all the limitations listed and discussed above. However, the truncated model is useful for obtaining conservative results to predict VIV response of a full-length model.

During the model test, the upper end of the SCR is attached to a mechanical oscillator that simulates the motion trajectories at the truncation point. It should be noted that the top truncation motion is the only excitation to the test SCR, there is no ocean current generated during the vessel motion-induced VIV model test. To measure the dynamic riser responses during the model test, fiber brag grating (FBG) strain sensors are instrumented along the entire riser at 25 stations. The numbering order is illustrated in Fig. 3, where station No.1 and No.25 have the distance of 1.05 m with respect to bottom and top end respectively, the rest stations have the same distance of 0.9 m with its adjacent stations. At each measuring station, there are four strain sensors around the riser cross section, two along the out-of-plane direction and the other two along the in-plane direction. Besides, there is a three-component force transducer measuring axial tension, drag and lift forces at the top end of the riser and a single-component force transducer measuring axial tension at the bottom end. During the tests, only the dynamic strains, end point forces and truncation point motion time histories are measured directly. They are synchronously recorded at a sampling frequency of 250 Hz, which is high enough to capture all the dynamic responses. Each test case last for the time of 20 vessel motion periods. Other parameters like riser in-plane, out-of-plane displacement or velocities are either based on numerical simulations or reconstructed from experimental measurements, which will be explained further in the later paragraphs. More detailed description regarding the model test design, scaling and truncation strategy can be referred to published literatures (Wang et al., 2014b, 2015b).

Table 1
Physical properties of the truncated model.

Item	Scaling Ratio	Full Scale (Full Length)	Full Scale (Truncated)	Model Scale (Measured)
Total Length (m)	λ	4010	456.53	23.71
Water Depth (m)	λ	1500	171.43	9
Hang-off Angle (°)	1	75	46.24	46.24
Length of Sag-bend (m)	λ	1809.12	401.53	21.0806
Horizontal Length of Flow Line (m)	λ	2200.88	55	2.626
Horizontal Length of Sag-bend (m)	λ	886.30	350.81	18.4175
Outer Diameter (m)	λ	0.4	0.4	0.024
Mass in Air (Kg/m)	$1.025\lambda^2$	234.49	234.49	0.69
Mass Ratio	1	1.82	1.82	1.53
Bending Stiffness *EI* (N m^2)	$1.025\lambda^5$	4×10^7	4×10^7	10.5
Tensile Stiffness *EA* (N)	$1.025\lambda^3$	4.14×10^9	4.14×10^9	6.67×10^5

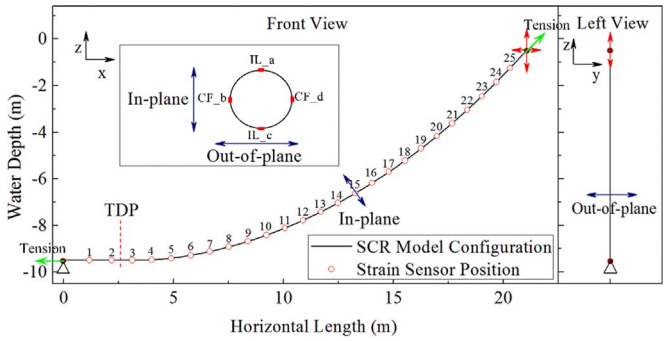

Fig. 3. Geometrical configuration of the truncated SCR test model and the strain sensor instrumentation.

3. Results and discussion

In total, there are 63 test cases carried out in the vessel motion-induced VIV model test with various combinations of the heave amplitude and period. Preliminary investigations have been carried out to understand the heave amplitude and period effects on vessel motion-induced VIV (Wang et al., 2014a). However, considering the fact that vessel motion-induced VIV is in fact oscillating current-induced VIV, *KC* number and maximum equivalent current velocity are supposed to be more appropriate as the governing parameters for vessel motion-induced VIV. It is expected that we should have proposed a non-dimensional parameter like reduced velocity

$$V_R = \frac{V_n}{f \cdot D} \tag{2}$$

where V_n is the local or global maximum equivalent current velocity upon different application, f can be the structure natural frequency or response frequency. Reduced velocity is a non-dimensional parameter describing the travelling length of the flow passing the structure during one vibration cycle. A good example of using reduced velocity is to identify the vortex shedding patterns for a rigid cylinder VIV in steady flow by Williamson and Govardhan(2004). Reduced velocity has also been adopted in our previous studies on a short cylinder VIV model test in oscillatory flow where VIV responses in most test cases are dominated by mode one (Fu et al., 2013a, 2013b). However, to the presented large-scale riser model test, VIV responses are expected to be more complex and varying significantly with different vessel motion parameters (Wang et al., 2014a, 2014b). We could have used the vessel motion frequency f_{im} or any of the riser natural frequency f_n to normalize the equivalent current velocity V_n. However, such normalization is a process only for the intention to obtain a non-dimensional parameter without practical physical meaning and it is not referable for other applications. A reasonable normalization is to use the VIV response frequency f_{resp} as f in Eq. (2). The dilemma is that f_{resp} is unknown before the model test, therefore, it is impossible to use f_{resp} for the normalization as well. Accordingly, we decide to use the maximum equivalent current velocity, which is a physical parameter and can be easily refer to the well-known ocean current velocity in the engineering application point of view, as one of the governing parameters for the following results and discussions.

In this paper, three groups of the test cases are selected for comparative study as listed in Table 2. According to the numerical simulations on the in-plane riser dynamic responses for these test cases in Orcaflex (Orcina, 2012) (a constant drag coefficient C_D=1.2 and a constant added mass coefficient C_a=1 are used), two cases in each group have approximately the same estimated maximum equivalent current velocity $V_{n,\max}$ along the entire riser. But, the maximum *KC* number $KC_{\max}$ for the two cases in the same group differs. $KC_{\max}$ can be defined as

$$KC_{\max} = \max(KC(s)) = \max\left(\frac{2\pi A_n(s)}{D}\right); \quad s \in (0, \quad L) \tag{3}$$

where, A_n is the riser in-plane normal motion displacement amplitude, and D is the outer diameter of the riser model, L is the length of the test SCR model.

In addition, as can be observed from Table 2, cases No.2 and No.3 have similar $KC_{\max}$, as do cases No.4 and No.5, which allows for comparisons of the maximum equivalent current velocity effect. It should be mentioned that the real riser in-plane motion might be a bit different than what we estimated, because the hydrodynamic coefficients, especially the drag coefficient, would be amplified (or varying) due to the existence of VIV. Since we do not have the direct measurements on the riser displacement, it's quite hard to reconstruct the riser in-plane motion from our measured strain because SCR in-plane global motion is a non-linear large displacement but small deformation problem, which would be an interesting topic in the near future.

3.1. In-plane riser dynamic responses

As mentioned, vessel motion-induced VIV occurs due to the existence of the equivalent oscillating current which is in fact generated by the riser in-plane motion relative to the still water. Therefore, before detailed discussions on vessel motion-induced VIV responses, the equivalent current distribution for the selected cases are studied first.

Fig. 4 illustrates that the local *KC* numbers have the similar distribution along the riser for all the six cases, where they increase from the bottom, reach the maximum value at the lower sag-bend region (near sensor No.10) and then gently decrease till the top end of the riser. The most distinctive difference among these cases is the peak *KC* number value $KC_{\max}$, particularly for the two cases in the same group in Table 2 (cases in the same group have the same line color in Fig. 4). It can be concluded from Fig. 4 that the *KC* number distribution and $KC_{\max}$ under the same type of vessel motion is mostly dependent on the vessel motion amplitude rather than the motion period as expected.

Fig. 5 illustrates the instantaneous equivalent current velocity distribution (estimated using Orcaflex) along the riser in the form of contour plots. Inside of each subplot, the first row illustrates the vessel motion time histories, where the red solid curve presents the vertical motion and the blue dashed curve represents the horizontal motion. Every subplot in Fig. 5 includes results for two vessel motion periods, and each motion period can be divided into two phases according to the vertical motion direction: 'lift-up' and 'push-down'. The second row (the contour plot) represents the in-plane time-varying equivalent oscillating current that normal to the riser axis. The magnitude of the equivalent current is denoted by the color variation according to the color map, which locates to the right of each contour plot. It should be noted that the contour plots have the same color map range for the two cases inside each group. Therefore, the comparison on the equivalent current distribution between two cases in one group would be more intuitive.

Similar to the local *KC* number distribution in Fig. 4, the instantaneous current velocities also increase from the bottom, reach the

Table 2
Test cases for analysis.

Group	*Case No.*	V_{n_max} (m/s)	KC_{max}	A_{im} (m)	T_{im} (s)	$Re_{\_max}$
A	1	0.28	39	0.105	3.21	6720
	2	0.27	74	0.21	5.96	6480
B	3	0.50	70	0.21	3.67	12000
	4	0.51	104	0.315	5.27	12240
C	5	0.59	102	0.315	4.81	14160
	6	0.61	120	0.37	5.50	14640

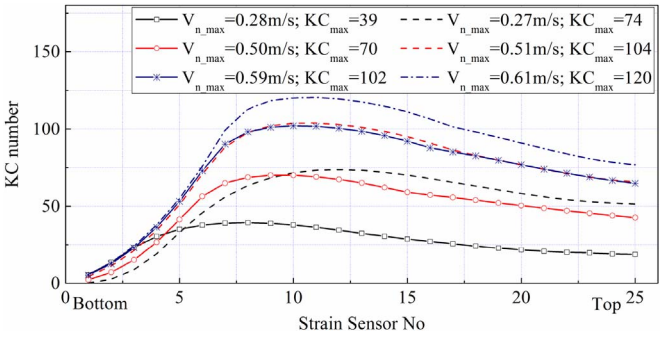

Fig. 4. Local *KC* number distribution along the riser for the six selected cases.

maximum velocity near strain sensor No.10 to No.15 and then generally decrease till the top end of the riser. Besides, the horizontal discrete contours in each subplot indicate that the current velocity has a periodical variation of incident direction with time. Another observation in Fig. 5 is that the local maximum current location in the 'lift-up' phase is always upper than that in the 'push-down' phase, as indicated by the arrows. This could lead to the difference in the associated VIV responses.

Based on the color variation in these contour plots, the zero velocity region (indicated by the white triangle area in the bottom of the contour plots) at the bottom of the riser reveals another phenomenon, known as touch down point (TDP) variation. A boundary line in these zero velocity region illustrates the TDP variation trajectory as indicated by the arrows. It can be summarized from the comparison in Fig. 5 that TDP variation becomes more significant with the increasing vessel motion amplitude. Such TDP variation further leads to the asymmetric distribution of the equivalent current between 'lift-up' and 'push-down' phase, and also lead to the riser effective sag bend length variation.

Generally speaking, the equivalent current distributions in all the three groups are quite similar in terms of the contour distribution. However, there are some local discrepancies for the cases in the same group. For example in Fig. 5(2) for the large $KC_{\max}$ case (case No.2), the current velocity at upper part of the riser is obviously higher. To summarize, it can be concluded that the equivalent current distribution is decided mostly by the maximum equivalent current velocity $V_{n.\max}$, in other word, it is decided by both vessel motion amplitude and period as expected.

3.2. Out-of-plane VIV strain and displacement

To evaluate the out-of-plane VIV responses, we compare the experimentally measured response strain and numerically reconstructed displacement among the six selected cases. The VIV strain can be calculated by Eq. (4) based on the strain measurement using FBG strain sensors:

$$\varepsilon_{CF.VIV}(s,t) = (\varepsilon_{CF.b}(s,t) - \varepsilon_{CF.d}(s,t))/2 \quad (4)$$

where $\varepsilon_{CF.b}(s,t)$ and $\varepsilon_{CF.d}(s,t)$ denote the original strain time series sampled at out-of-plane locations CF_b and CF_d, as illustrated in Fig. 3. The out-of-plane VIV displacement is then reconstructed based on mode superstition method (Wang et al,, 2015b).

Fig. 6 demonstrates the out-of-plane vessel motion-induced VIV strain in the form of contour plot. Inside each subplot, the first row represents the vessel motion time histories. The second row represents the measured riser top tension time histories. The third row illustrates the instantaneous VIV strain distribution along the riser with the time evolvement. It should be mentioned that the color map ranges for the two contour plots in each group are the same, in order to have a more straightforward comparison. It can be summarized from each subplot that vessel motion-induced VIV is originated from the middle part of the riser and then propagates toward both sides of the riser in the form of travelling waves, as indicated by the arrows in the contour plots. There are also some standing waves at ends of the riser because of the mix of travelling waves and end reflecting waves. What's more, there are quite significant differences between the instantaneous strain distributions in the 'lift-up' and 'push-down' phases, which are strongly correlated to the local equivalent current distributions as presented in Fig. 5 and the tension variation. As has been explained in the published literature (Wang et al., 2015b), larger tension during 'lift-up' would lead to a higher natural frequency but a lower response mode. On the contrary, smaller tension during 'push-down' would lead to a lower natural frequency but a higher response mode. In the model test, relatively larger responses are witnessed near the top end for both cases. Yet, to a full-length SCR, the upward travelling waves would continue to travel up without any block from the truncated top end. The hydrodynamic damping above the truncation point would be sufficient to damp the travelling energy before reflecting from the real top end of the full-length SCR. From this point of view, the truncated model in the present work is not fully presenting the VIV as in a full-length riser. But since there are additional reflecting waves affect from the top truncated end, we believe that this makes the result to become the upper bound of the VIV in a full-length SCR.

Fig. 7 presents the measured out-of-plane VIV responses in terms of statistical values including maximum and RMS responses (strains and A/Ds) for the selected test cases. It should be mentioned that each test case lasts for the time of 20 vessel motion periods, and we have calculated the maximum and RMS values for strain and A/D for each period in the 18 periods in between (data in the first and last period are not included). The statistical values in Fig. 7 are the averaged ones from the 18 periods to be more general and representative. The strain comparisons for each group are on the left and A/Ds are on the right of Fig. 7. What's more, strain measurements for case No.2 are integrated in Fig. 7(3) as illustrated by the blue curves, and results for case No.4 are integrated in Fig. 7(5), as illustrated by the blue curves, to reveal theV_{n_max} effects.

Based on the comparisons on the statistical VIV responses for the two cases in group A, clear discrepancies can be witnessed in terms of both strains and A/Ds. VIV responses for the large KC_{max} case are larger than the small KC_{max} case. There are three possible reasons for these discrepancies:

1) The *KC* number effect: If we refer to what we observed for VIV under small *KC* number oscillatory flow for a rigid cylinder or short straight model. The RMS VIV responses under small *KC* number would be slightly larger than that with the same maximum current velocity but larger *KC* number. Because for a straight cylinder, *KC* number is the same along the whole structure and VIV response under small *KC* number is less time-varying and the responses are more stable (Sumer and Fredsøe, 1988; Fu et al., 2013a). However, to a SCR, the local *KC* number also varies quite much due to its geometric configuration, as has been explained in Fig. 4. The KC_{max} for case No.1 is the smallest at 39, approximately half of that for case No.2. The local *KC* numbers are much smaller, refer to Fig. 4. It is assumed that the locally varying small *KC* numbers make the VIV responses to be less developed compared to the large KC_{max} case. A similar decreasing trend of VIV response amplitude with decreasing *KC* number was also reported by Rateiro where in his model test, all KC_{max} are below 30.

2) The local in-plane normal velocity profile: as shown in Figs. 5(2), the local equivalent current velocity for a large KC_{max} case (case No.2) is higher at the top of the riser compare to that in Fig. 5(1), and possibly a higher or more stable mode is excited for the large KC_{max} case.

3) TDP variation: The top motion is greater for a large KC_{max} case (case No.2), which causes more of the riser to be lifted, thus leading to a larger response at the lower end for a large KC_{max} case, which agrees with the observations.

The RMS responses for the two cases in group B illustrated by the black and red dashed curves from second row in Fig. 7, are almost

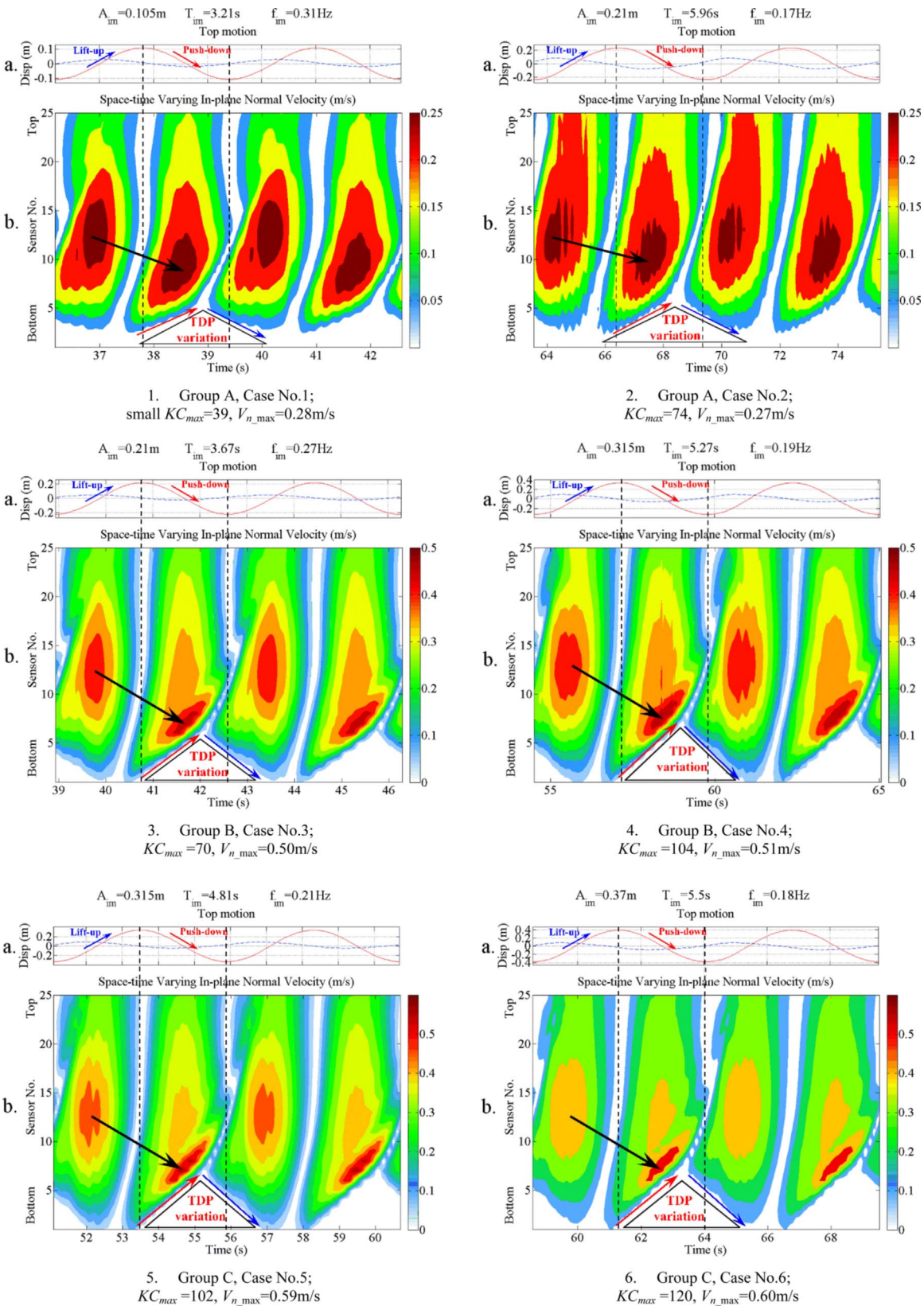

Fig. 5. Estimated instantaneous in-plane equivalent current velocity distribution for the six selected cases (in each subplot, row a: top motion (dashed line—horizontal motion; solid line—vertical motion); row b: calculated instantaneous in-plane normal velocity).

identical. The match is also witnessed in group C from the third row in Fig. 7. These indicate the dominance of maximum equivalent current velocity on vessel motion-induced VIV, typically for the cases when KC_{max} is sufficiently large. The slight discrepancy for the maximum A/D and strain is understandable considering the time-varying nature and randomness of vessel motion-induced VIV.

Next, we compare the responses for the two cases with the same KC_{max} but different maximum equivalent current velocity, as indi-

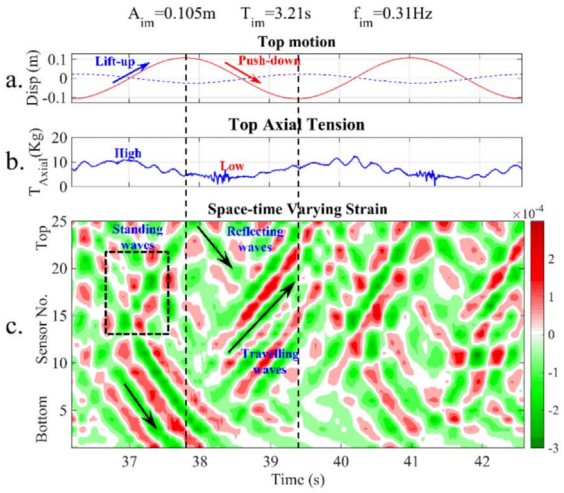

1. Group A, Case No.1;
small KC_{max}=39, V_{n_max}=0.28m/s

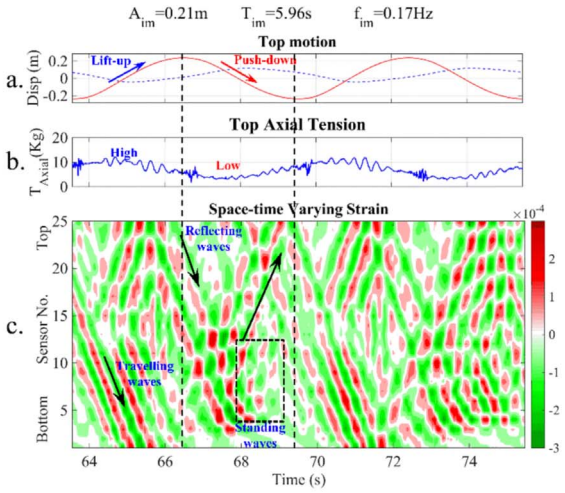

2. Group A, Case No.2;
KC_{max}=74, V_{n_max}=0.27m/s

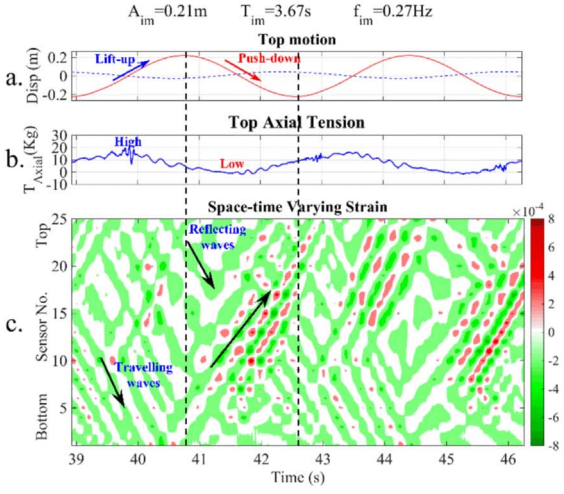

3. Group B, Case No.3;
KC_{max} =70, V_{n_max}=0.50m/s

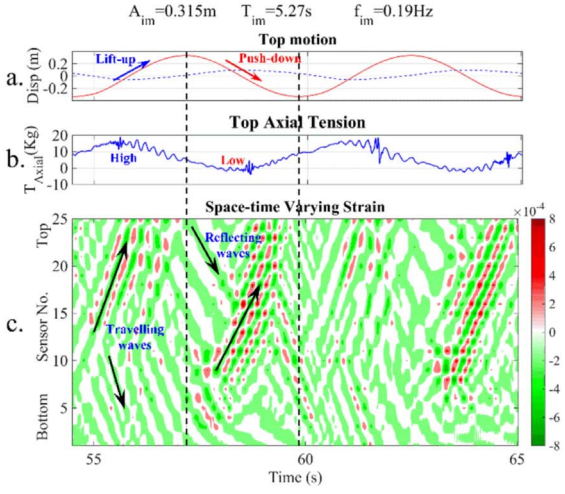

4. Group B, Case No.4;
KC_{max} =104, V_{n_max}=0.51m/s

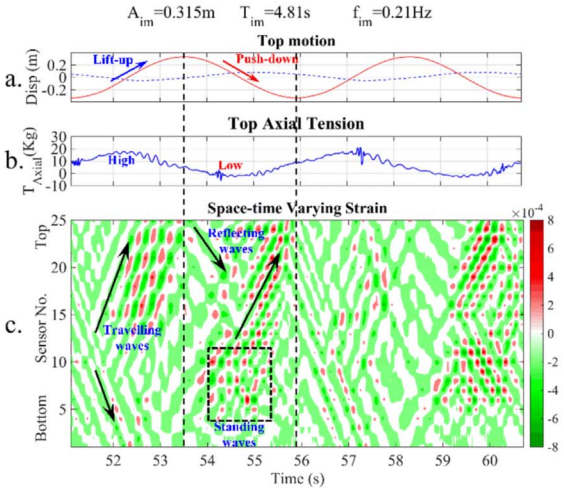

5. Group C, Case No.5;
KC_{max} =102, V_{n_max}=0.59m/s

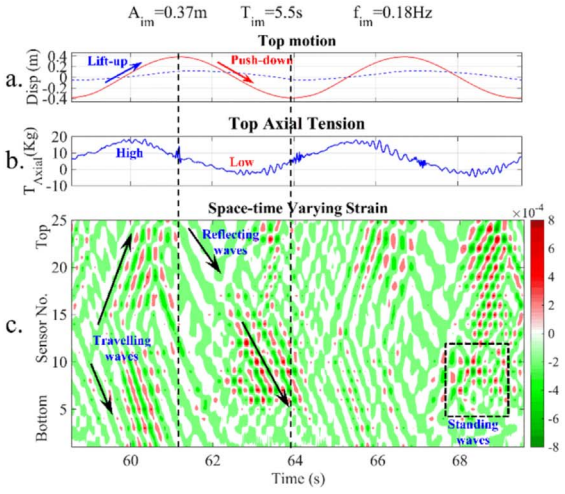

6. Group C, Case No.6;
KC_{max} =120, V_{n_max}=0.60m/s

Fig. 6. Out-of-plane space-time varying strain for the six selected cases (in each subplot, row a: top motion time history (dashed line—in-plane horizontal motion; solid line—in-plane vertical motion); row b: top axial tension variation; row c: space-time varying strain).

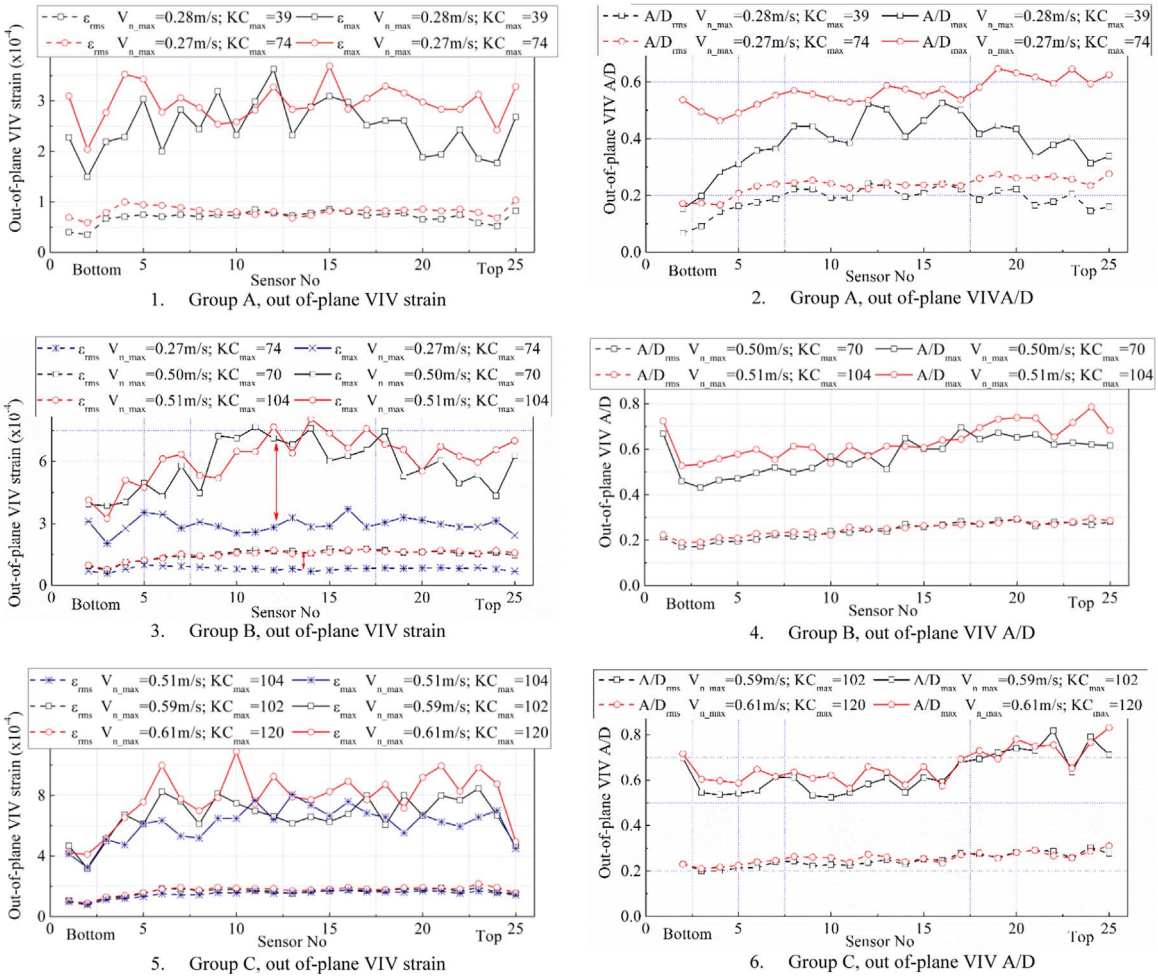

Fig. 7. Out-of-plane vessel motion-induced VIV strain and A/D for the three groups (left: strain; right: A/D).

cated by the black and blue curves in Figs. 7(3) and (5). In Fig. 7(3), there is a distinct difference in both maximum and RMS strain responses, as marked with the arrows, whereas in Fig. 7(5), the difference is visible but quite minor. It can be summarized that these VIV response differences are strongly corresponding to the maximum equivalent current velocity: A higher equivalent current velocity is expected to excite higher natural mode accompanied by larger strain amplitudes. As listed in Table 2, the maximum equivalent current velocity in case No.2 is nearly half of that in case No.3, but cases No.4 and No.5 have quite similar maximum velocities.

In general, if the KC_{max} is sufficiently large (at least about 39 according to the present study), the out-of-plane vessel motion-induced VIV response, especially the statistical values including the maximum and RMS strain (A/D), depends on the maximum equivalent current velocity and is independent of the KC_{max} nor the local KC number distribution. However, for small KC_{max} cases, the response depends on the maximum equivalent current velocity, KC_{max} and the local KC number distribution.

3.3. Out-of-plane VIV response frequency

Based on the previous understandings on vessel motion-induced VIV, it is known that the response frequency of vessel motion-induced VIV would vary with time and riser location as a result of the space- and time-varying equivalent current velocity distribution, as well-demonstrated in Fig. 5. By assuming there is only one dominant frequency for each measuring station at any given time instant, contour plots illustrating the instantaneous dominant response frequency distributions are established for each test case by wavelet analysis technique (Wang et al., 2015b), as shown in Fig. 8. It should be mentioned that the frequency range of the contour plots for the two cases in the same group is the same, in order to have a clearer comparison. These graphs show that the dominant response frequency for vessel motion-induced VIV experiences a distinct space- and time-variation, which is quite different from that for steady-current-induced VIV, as expected.

Specifically, from the comparison on the response frequency distribution for the two cases in Figs. 8(1) and (2), it can be seen that the response frequency for the small KC_{max} case is generally higher and more consistent with time. Firstly, this is because there are no enough distance or time for the VIV responses to be damped for case No.1 when KC_{max} and local KC number are much smaller. Moreover, small local KC number would allow the riser to enter its own wake when it reversed direction (in short, we can call this the own-wake effect (Wang et al., 2015b). The other five cases have higher KC_{max} and therefore have similar dominant frequency distributions, where the response frequencies seem to be more consistent along the length of the riser but varying significantly over time. The instant frequency is typically low when the riser reaches its vertical top location when the top vessel motion velocity is close to zero, for example, when t=66.5 s in Fig. 8(2). However, the low response frequency time window is not repeated when the riser reaches its vertical bottom location (t=69.5 s in Fig. 8(2)). This local response frequency asymmetry is assumed to be correlated with the top tension variation as well.

According to previous investigation on the response frequency for vessel motion-induced VIV. One representative dominant frequency

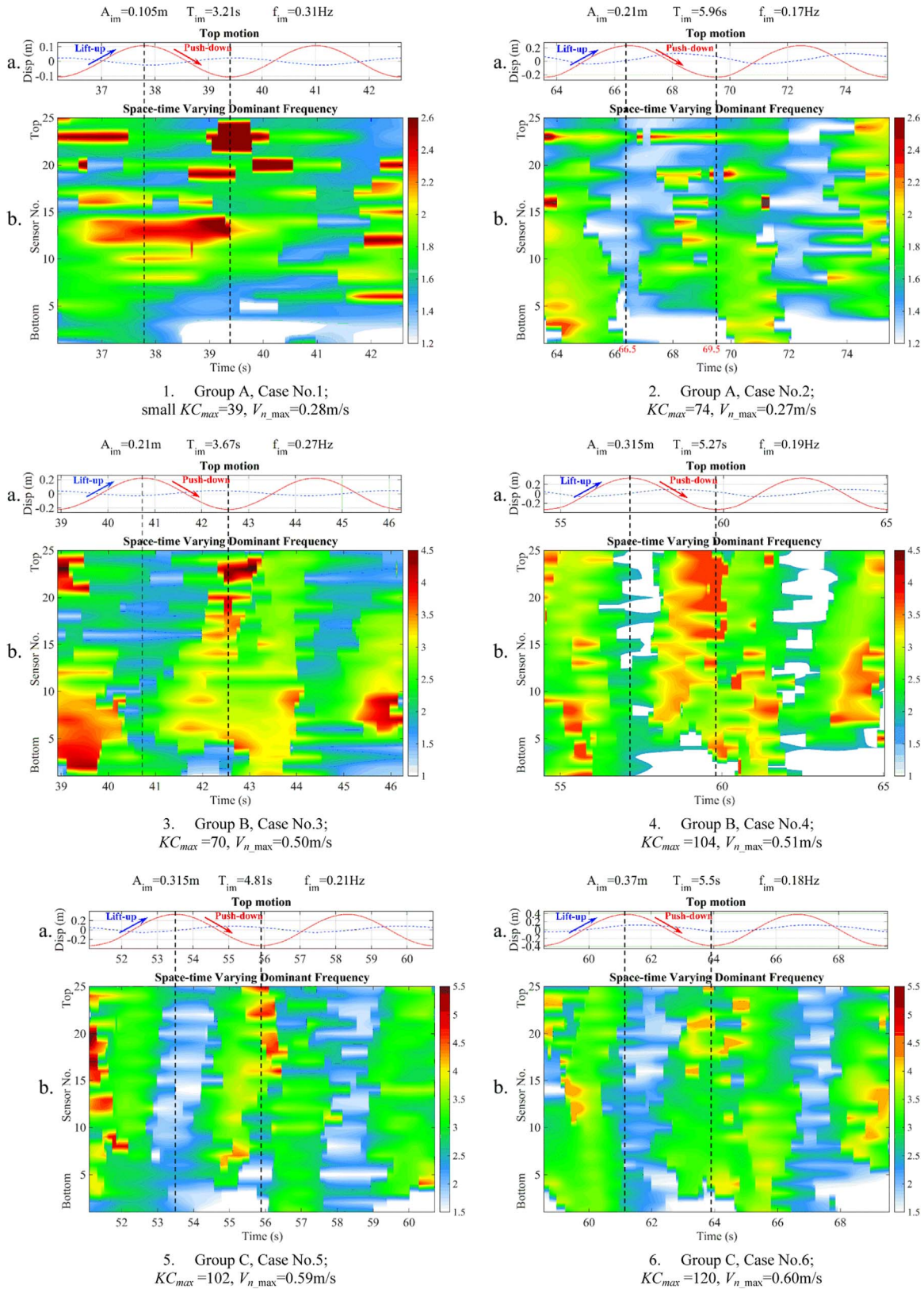

Fig. 8. Out-of-plane VIV response frequency distributions (in each subplot, row a: top motion time history (dashed line—in-plane horizontal motion; solid line—in-plane vertical motion); row b: space-time varying dominant frequency).

f_{domi} can be further obtained from the general frequency spectrum for each test case (Wang, 2015b), and the identified dominant frequency is found to have a linear Strouhal relationship with the maximum equivalent current velocity, as expressed by Eq. (5).

$$St = \frac{f_{domi} \cdot D}{V_{n.\max}} = 0.14 \tag{5}$$

where St is the equivalent Strouhal number governing the dominant

frequency of vessel motion-induced VIV. $St = 0.14$ is an important observation that can be used in future VIV response prediction.

A further attempt is to investigate the frequency ratio between the out-of-plane VIV response frequency and the in-plane vessel motion frequency. The frequency ratio indicates the vortex shedding pairs N per vessel motion period for each case (this is directly related to the contour color variation within one motion period in Fig. 6). The summarized vortex shedding pairs in Table 3 indicate that N satisfies an integral relationship with KC_{max} as

$$N = \frac{f_{domi}}{f_{im}} = St \cdot KC_{\max} \tag{6}$$

In fact, the frequency relationship in Eq. (6) is especially important for the test cases when $KC_{\max}$ is even smaller than what we presented in this paper ($KC_{\max} = 39$). In such cases, a constant equivalent Strouhal number (for our test model, $St = 0.14$) may fail to determine the dominant response frequency. Nevertheless, the integral relationship $N = f_{domi}/f_{im}$ is always valid (N varies with different KC number range). This has been reported by Fernandes et al. (2012) for rigid cylinder test, by Rateiro (2013) for the SCR model test, and by Wang et al. (2016) for the free-hanging riser model tests.

To summarize, for vessel motion-induced VIV, there is always an integral relationship between the VIV response frequency and vessel motion frequency. When KC_{max} is sufficiently large (at least about 39 according to the present study), the response frequency exhibits more time-varying features, and the dominant frequency follows the equivalent Strouhal relationship when $St = 0.14$. For the small KC_{max} cases, the VIV response frequency varies less over time because of the small KC number effects, i.e., shorter time windows for damping and own-wake effects.

3.4. Fatigue damage caused by vessel motion-induced VIV

Combining VIV response amplitude and response frequency, fatigue damage is a more comprehensive and straightforward parameter to evaluate the VIV effects. Besides, fatigue damage is also an important riser design criteria that should always be satisfied (DNV, 2010b). Therefore, in this section, fatigue damage caused by vessel motion-induced VIV is discussed and compared among the six selected test cases. Based on the rain-flow counting, measured VIV responses can be firstly converted from time histories into stress cycles (Amzallag et al., 1994), and then The **B1** curve from DNV (2010b) was applied in the fatigue damage analysis. The curve chosen is valid for the corrosion-free specimens in seawater. The parameters adopted in this study are listed in Table 4. Miner fatigue accumulation method is used to calculate the fatigue damage at each measuring station. Detailed procedures related to this fatigue damage calculation methodology based on experimental measurements can be found in the published literature (Wang et al., 2014b).

Fig. 9 presents the fatigue damage distribution along the riser caused by out-of-plane vessel motion-induced VIV for the six cases. Similar to the statistical strains and A/Ds, the fatigue damage is also almost irrelevant to KC_{max} when KC_{max} is sufficiently large (at least about 39 according to the present study), as illustrated by the fatigue damage comparison in groups B (by red curves) and C (by blue curves) in Fig. 9.

However, in group A (by black curves), the fatigue damage for the large KC_{max} case is considerably greater than that for the small KC_{max} case even though the response frequency in the small KC_{max} case is higher and less time-varying according to that observed in Fig. 8. The reason for this discrepancy is that the fatigue damage is exponentially related to the stress amplitude but linear with the number of stress cycles (in other words, the response frequency), which is given by the definition of the S-N curve (DNV, 2010b). The stress amplitude is higher for the large KC_{max} case, as shown in Fig. 7(1), which accordingly causes a notable difference in the fatigue damage for the cases in group A.

To summarize, if KC_{max} is sufficiently large (at least about 39 according to the present study), fatigue damage caused by vessel motion-induced VIV depends on the maximum equivalent current velocity and is independent of KC_{max}. However, for small KC_{max} cases, the fatigue damage depends on both the maximum equivalent current velocity and KC_{max}.

3.5. Top tension variation

In addition to the in-plane motion and out-of-plane VIV, vessel motion can also lead to substantial top tension variation to the attached SCRs. Riser top tension variation is also an essential parameter in the riser design and offshore operation. Generally speaking, for a riser subjected to vessel motion, there are three major contributions to the top tension variation:

1) The quasi-static geometry variation, which can be calculated based on the catenary equation and current vessel position;
2) The in-plane hydrodynamic forces due to the riser motion in still water (including drag and inertial terms);
3) The in-plane and out-of-plane hydrodynamic forces due to VIV (including the drag and inertial terms in both directions; VIV is known to significantly amplify the drag (Huang et al., 2011)), such hydrodynamic coefficients identification under vessel motion-induced VIV will be studied in the future.

Fig. 10 presents the tension variation comparison for the six cases. For each test case, the black block represents the quasi-static tension variation due to geometry changes; the patterned block represents the dynamic tension variation due to both geometry changes and in-plane hydrodynamic loads, which is calculated using Orcaflex neglecting VIV effects; and the red block represents the real tension variation measured during the model test, as has been presented in Fig. 6.

Based on the comparison, it can be seen that the variation in the quasi-static tension is rather small compared with that of the dynamic tension regardless of whether the VIV effects are included. Meanwhile, Fig. 10 shows that the VIV significantly contributes to the tension variations, almost doubles the tension variation by the state-of-the-art numerical simulation results.

Furthermore, the tension variation is quite close for the two cases inside each group, indicating the top tension variation is dominated by maximum in-plane equivalent current velocity. As stated previously from Fig. 5, the two cases in each group have similar maximum equivalent current velocities (velocity is related to the drag force) but different displacements (displacement is related to KC number, and then related to the geometry change) and different accelerations (acceleration is related to the inertial force). This further suggests that the tension variation is largely due to the drag force variation. Meanwhile, the clear differences between cases with similar KC_{max} (e.g., cases No. 2 and No.3 or cases No.4 and No.5) demonstrated the insignificance of the KC_{max} effect on tension.

Table 3
Vortex shedding pairs for selected test cases.

Group	*Case No.*	V_{n_max} (m/s)	KC_{max}	f_{im}	f_{domi}	N
A	1	0.28	39	0.31	1.89	6
	2	0.27	74	0.17	1.67	10
B	3	0.50	70	0.27	3.07	11
	4	0.51	104	0.19	2.91	15
C	5	0.59	102	0.21	3.10	15
	6	0.61	120	0.18	3.13	17

Table 4
S-N curve parameters.

S-N curve	log $\bar{a}$	m
B1	12.436	3.0

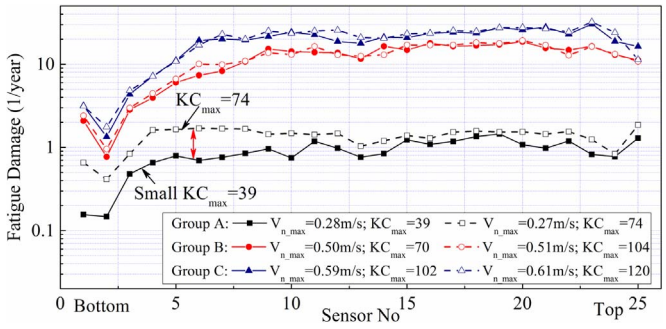

Fig. 9. Fatigue damage distribution caused by out-of-plane vessel motion-induced VIV.

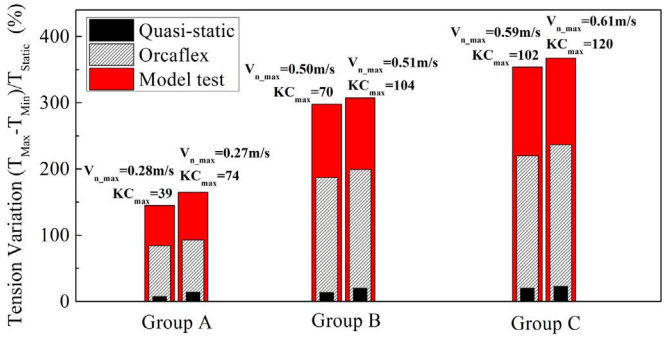

Fig. 10. Tension variations from quasi-static analysis, simulations and experimental measurements.

To summarize, the estimated maximum equivalent current velocity is the dominant parameter affecting the SCR top tension variation, and the presence of vessel motion-induced VIV would significantly amplify the tension variation.

4. Conclusions

In this paper, we select six representative test cases from the SCR model test campaign for comparative studies, in order to further our understandings on the dominant parameters for vessel motion-induced VIV. Instantaneous and statistical VIV responses including VIV strains, A/Ds, response frequency, fatigue damage and top tension variation were discussed and compared.

Results indicate that the general out-of-plane VIV responses, fatigue damage and tension variation depend most strongly on the estimated maximum equivalent current velocity V_{n_max}. It is independent on the maximum KC number KC_{max} when KC_{max} is sufficiently large (at least about 39 according to the present study, it should be mentioned that the riser in-plane motions are estimated numerically using C_D=1.2, the limit KC_{max}=39 we conclude here might be subjected to minor change considering real in-plane motion). For small KC_{max} cases, the VIV responses are significantly affected by the small KC number and local KC number effect, which cause the responses to be less developed and less time-varying. The small KC number effect is caused by limited excitation and damping cycles and also by the riser passing through its own wake. The maximum equivalent current velocity is also found to be the dominant parameter for the top tension variation. The response frequency model for vessel motion-induced VIV is also reviewed including an integral frequency ratio and an equivalent Strouhal number $St = 0.14$. The equivalent Strouhal number is valid especially for the cases when KC_{max} is large enough. The VIV response frequency models are useful for the future VIV prediction model development.

Generally speaking, the results of the present study suggest that the maximum equivalent current velocity is an effective parameter governing the general vessel motion-induced VIV responses but only when KC_{max} is sufficiently large. Vessel-motion-induced VIV for low KC_{max} is more complex and strongly affected by the small KC number and local KC number effects. Because small KC numbers are more common to a fatigue sea state, further research on vessel motion-induced VIV at small KC numbers is recommended. According to the present research conclusions, it is believed that other type vessel motions would also lead to significant VIV to the SCR whenever there are equivalent oscillating current around the riser. Moreover, vessel motion-induced VIV for other type of risers like steel lazy-wave riser, free-hanging riser should also be evaluated in the future.

Acknowledgements

The authors gratefully acknowledge the financial support from Statoil, Norway (Contract Nos. 4502203831, 4502933986), for this research (under the “VIV Effects in Sag-bends of SCRs” program). The authors would also like to thank Statoil for permission to publish the data from this research. Support from the National Science Foundation of China is also greatly appreciated (Grant No. 51490674).

References

Amzallag, C., Gerey, J.P., Robert, J.L., Bahuaud, J., 1994. Standardization of the rainflow counting method for fatigue analysis. Int. J. Fatigue 16, 287–293.
Baarholm, G.S., Larsen, C.M., Lie, H., 2006. On fatigue damage accumulation from in-line and cross-flow vortex-induced vibrations on risers. J. Fluid Struct. 22, 109–127.
Basim, B.M., 2001. New frontiers in the design of steel catenary risers for floating production systems. J. Offshore Mech. Arct. Eng. 123 (4), 153–158.
Chaplin, J.R., Bearman, P.W., Huera, H.F.J., Pattenden, R.J., 2005. Laboratory measurements of vortex-induced vibrations of a vertical tension riser in a stepped current. J. Fluid Struct. 21, 3–24.
Cunff, C.L., Biolley, F., Damy, G., 2005. Experimental and numerical study on heave-induced lateral motion (HILM). In: Proceedings of the 24th OMAE, Halkidiki. Paper No. OMAE2005-67019.
DNV, 2010a. DNV-RP-F205: Global Performance Analysis of Deepwater Floating Structures. Det Norske Veritas.
DNV, 2010b. DNV-RP-C203: Fatigue Design of Offshore Steel Structures. Det Norske Veritas.
Fernandes, A.C., Mirzaeisefat, S., Cascão, L.V., 2014. Fundamental behavior of Vortex Self Induced Vibration (VSIV). Appl. Ocean Res. 47, 183–191.
Fernandes, A.C., Silva, E.M.C., Franciss, R., Coelho, F.M., Neto, S.F.S., 2008. VSIV (vortex self-induced vibration) kinematics. In: ASME of 27th International Conference on Ocean, Offshore and Arctic Engineering, Estoril. Paper No. 2008-57579.
Fernandes, A.C., Sefat, S.M., Cascão, L.V., Franciss, R., 2012. Analysis of PIV tests results of the Vortex Self Induced Vibration (VSIV) of a cylinder. In: ASME of 31st International Conference on Ocean, Offshore and Arctic Engineering, Rio de Janeiro. Paper No. 2012-84021.
Fu, S., Wang, J., Baarholm, R., Wu, J., Larsen, C.M., 2013. Features of vortex-induced vibration in oscillatory flow. J. Offshore Mech. Arct. Eng. 136 (1), 011801.
Fu, S., Wang, J., Baarholm, R., Wu, J., Larsen, C.M., 2013b. VIV of flexible cylinder in oscillatory flow. In: Proceedings of the 32nd OMAE, Nantes. Paper No. 2013-10348.
Gonzalez, E.C., 2001. High Frequency Dynamic Response of Marine Risers with Application to Flow-induced Vibration (Ph.D. dissertation). Massachusetts Institute of Technology, Cambridge, MA, USA.
Grant, R.G., Litton, R.W., Mamidipuli, P., 1999. Highly compliant rigid (HCR) riser model tests and analysis. In: Proceedings of the OTC. Paper No. 10973.
Griffin, O.M., Vandiver, J.K., 1984. Vortex-induced strumming vibrations of marine cables with attached masses. J. Energ. Resour. Technol. 106, 458–485.
Huang, S., Khorasanchi, M., Herfjord, K., 2011. Drag amplification of long flexible riser models undergoing multi-mode VIV in uniform currents. J. Fluid Struct. 27 (3), 342–353.
Liao, J.C., 2002. Vortex-induced Vibration of Slender Structures in Unsteady Flow (Ph.D. dissertation). Massachusetts Institute of Technology, Cambridge, MA, USA.
Lie, H., Kaasen, K.E., 2006. Modal analysis of measurements from a large-scale VIV model test of a riser in linearly sheared flow. J. Fluid Struct. 22, 557–575.
Orcina, 2012. OrcaFlex Manual, Version 9.5d. UK.
Quéau, L.M., 2015. Estimating the Fatigue Damage of Steel Catenary Risers in the Touchdown Zone (Ph.D. dissertation). The University of West Australia, Crawley, WA, Australia.
Rateiro, F., Gonçalves, R.T., Fujarra, A.L.C., Mendes, P., 2012. Risers model tests:

Scaling methodology and dynamic similarity. In: Proceedings of the 22nd International Offshore and Polar Engineering Conference. International Society of Offshore and Polar Engineers, Rhodes. Paper No. ISOPE-I-12-307.

Rateiro, F., Gonçalves, R.T., Pesce, C.P., Fujarra, A.L.C., Franzini, G.R., Memdes, P.A., 2013. Model scale experimental investigation on vortex self induced vibrations (VSIV) of catenary risers. In: Proceedings of the 32nd OMAE, Nantes. Paper No. OMAE2013-10447.

Sumer, B.M., Fredsøe, J., 1988. Transverse vibrations of an elastically mounted cylinder exposed to an oscillatory flow. J. Offshore Mech. Arct. Eng. 110, 387–394.

Tognarelli, M.A., Slocum, S.T., Frank, W.R., Campbell, R.B., 2001. VIV response of a long flexible cylinder in uniform and linearly sheared currents. In: Proceedings of the OTC. Paper No. 16338.

Trim, A.D., Braaten, H., Lie, H., Tognarelli, M.A., 2005. Experimental investigation of vortex-induced vibration of long marine risers. J. Fluid Struct. 21, 335–361.

Vandiver, J.K., Marcollo, H., Swithenbank, S., Jhingran, V., 2005. High mode number vortex-induced vibration field experiments. In: Proceedings of the OTC. Paper No. 17383.

Wang, J., Fu, S., Baarholm, R., 2014a. Vortex-induced vibration of steel catenary riser under vessel motion. In: Proceedings of the 33rd OMAE, San Francisco. Paper No. 2014-23584.

Wang, J., Fu, S., Baarholm, R., Wu, J., Larsen, C.M., 2014. Fatigue damage of a steel catenary riser from vortex-induced vibration caused by vessel motions. Mar. Struct. 39, 131–156.

Wang, J., Fu, S., Baarholm, R., Wu, J., Larsen, C.M., 2015a. Fatigue damage induced by vortex-induced vibrations in oscillatory flow. Mar. Struct. 40, 73–91.

Wang, J., Fu, S., Baarholm, R., Wu, J., Larsen, C.M., 2015b. Out-of-plane vortex-induced vibration of a steel catenary riser caused by vessel motions. Ocean Eng. 109, 389–400.

Wang, J., Xiang, S., Fu, S., Cao, P., Yang, J., He, J., 2016. Experimental investigation on the dynamic responses of a free-hanging water intake riser under vessel motion. Mar. Struct. 50, 1–19.

Williamson, C.H.K., Govardhan, R., 2004. Vortex-induced Vibrations. J. Fluid Mech. 36, 413–455.